A Fluid-Dynamic Based Approach to Reconnect the Retinal Vessels in Fundus Photography*

Francesco Calivá*[1], Andrew Hunter[1], Piotr Chudzik[1], Giovanni Ometto[2], Luca Antiga[3], Bashir Al-Diri[1]

***Abstract*— This paper introduces the use of fluid-dynamic modeling to determine the connectivity of overlapping venous and arterial vessels in fundus images. Analysis of the retinal vascular network may provide information related to systemic and local disorders. However, the automated identification of the vascular trees in retinal images is a challenging task due to the low signal-to-noise ratio, nonuniform illumination and the fact that fundus photography is a projection on to the imaging plane of three-dimensional retinal tissue. A zero-dimensional model was created to estimate the hemodynamic status of candidate tree configurations. Simulated annealing was used to search for an optimal configuration. Experimental results indicate that simulated annealing was very efficient on test cases that range from small to medium size networks, while ineffective on large networks. Although for large networks the nonconvexity of the cost function and the large solution space made searching for the optimal solution difficult, the accuracy (average success rate = 98.35%), and simplicity of our novel approach demonstrate its potential effectiveness in segmenting retinal vascular trees.**

I. INTRODUCTION

Recent studies have shown that both systemic and local disorders (e.g. diabetes, stroke and diabetic retinopathy) can alter both geometry and hemodynamic conditions in the retinal vasculature [1] [2] [3]. However, identification and quantification of such changes are challenging tasks since the retina is extremely heterogeneous and, as a consequence low signal-to-noise ratio, nonuniform illumination and contrast shifts in the images complicate the automated detection and analysis of geometrical changes. The latest segmentation algorithms produce highly accurate vessel segmentations [4] [5] [6] [7]. Nevertheless, the identification of the mutually overlapping venous and arterial trees is a nontrivial problem. Some automated segmentation methods segment vessels out as individual unconnected segments. It is not uncommon to extract broken segments, and crossing between vein and artery may be confused with a bifurcation of a single vessel, particularly where several bifurcations and crossings lie close together. Our novel approach determines the blood vessel connectivity based on the estimation of hemodynamic parameters, which cannot be directly measured from fundus images. In this paper, a zero-dimensional (0-D) model and a fluid-dynamics based cost function were created to simulate the hemodynamics in the vascular network and reconnect disconnected vascular segments (Sherman *et al.* [8]). To the best of our knowledge, this is the first study to use hemodynamic principles to determine vessels' connectivity.

[1] School of Computer Science, University of Lincoln, Lincoln (UK)
[2]Department of Ophthalmology, Aarhus University Hospital (Denmark)
[3]Orobix srl, Bergamo (Italy)

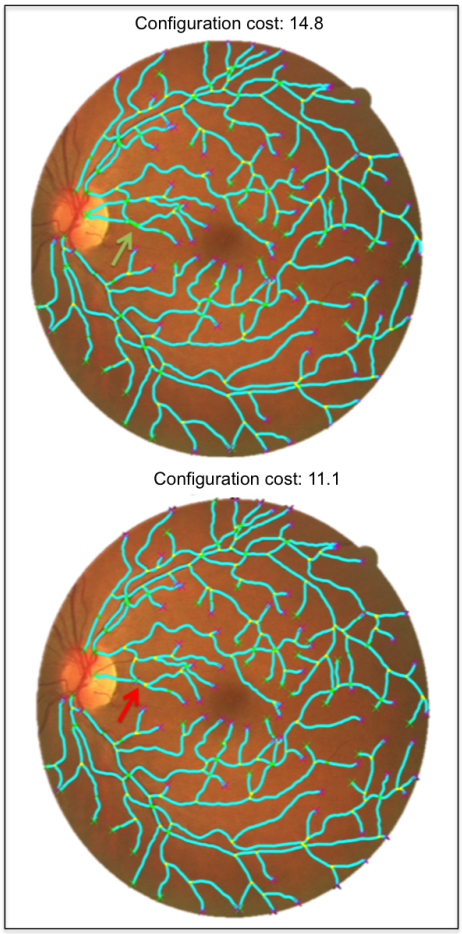

Fig. 1: The proposed framework's results for an exemplary fundus photography (DRIVE test set image 1). **Top**: The correct configuration derived by visually inspecting the artery/vein ground truth [9]. The green arrow points towards a bifurcation and a vessels crossing that were not correctly recognized in our optimal configuration (red arrow in the image located at the bottom part). **Bottom:** The less expensive configuration according to our cost function when a set of manually generated configurations were evaluated.

A. LITERATURE REVIEW

Among the most recent and relevant studies, Favali *et al.* [10] were inspired by the concept of association field that is implemented in the primary visual cortex and presented a connectivity algorithm based on the intuition that at the arteriovenous crossing a continuity in vessels' direction and

intensity exists. Estrada *et al.* [11] proposed a novel graph-theoretic approach, in which first a planar graph representative of the vasculature is extracted. An efficient search algorithm explores the solutions space and eventually provides the vascular topology and the final artery and vein labeled trees. Hu *et al.* [12] proposed a global three-step framework. It starts with the generation of an over-connected vessels network. A graph-based meta-heuristic algorithm disambiguates such network and, eventually, each tree is classified as arterial or venous by calculating the likelihood of each pixel of the centerline belonging to an artery or a vein.

II. MATERIALS AND METHODS

Our method was created using the publicly available DRIVE dataset [13]. This contains 40 fundus images obtained in the course of a diabetic retinopathy screening program in the Netherlands. Morphological skeletonization was applied on the first manual vessel reference standards to obtain the centerline of the vasculature. Our aim is to reconnect disconnected vascular segments and reconstruct the retinal vascular network. Each segment has two endpoints ($Send_i$ with $i \in \{1, 2\}$). We assumed that a segment-end can remain unconnected (terminal), or can be connected to one or two other segment-ends to form a bridge or a bifurcation respectively. All the segments-ends found within a circular area with radius of 14 pixels were identified as the end-candidates, to which a segment-end could be connected.

A. Retinal blood flow mechanics

The use of a fluid-dynamics based cost function provides with a framework to reconstruct a graph representative of the retinal vascular system. To simulate the fluid-dynamic conditions within the network, a simple 0-D electrical lumped elements model was designed (Fig. 2), and for simplicity the blood treated as a Newtonian fluid. Under this assumption the blood flow follows Hagen-Poiseuille's law (H-P). H-P flow expresses the relationship between pressure drop (ΔP) and blood flow through a tube (Eq. (1)).

$$\Delta P = R \cdot Q \tag{1}$$

In Eq. (1), $R = \frac{8\mu L}{\pi r^4}$ is the resistance that the blood encounters when flowing in a tube of radius r and length L, with $\mu = 0.04P$ being the blood viscosity. $G = \frac{1}{R}$ is the conductance of a vessel. The method devised in this paper solves an optimization problem, which aims at finding the best connection among segments. This is solved by iteratively evaluating an objective function, which includes fluid-dynamic terms. This framework is inspired by the intuition that the global minimum of our cost function is found with the correct network, since our cost function follows the fluid-dynamic principles behind the generation of vascular networks.

B. The objective function

The objective function was designed to replicate some of the biological hypotheses that guide the generation of a Murray's system. These are branching networks where a vessel splits into two branches and follows the principle of optimality which ensures the "fastest" transport, in terms of e.g. amount of oxygen per unit time, by the least amount of work needed as described by Murray's law [14] [15]. Therefore, in an optimal system, the total flow is transported by a set of vessels whose radii's cube sum to a constant value at each part of the network (Eq.(2)).

$$r_0^3 = \sum_{i=1}^{N} r_i^3 \tag{2}$$

Eq. (2) refers to a bifurcation, r_0 is the radius of the parent vessel, and r_i the radius of the i-th child. Furthermore, with regard to [14], volumetric flow through a tube is proportional to the radius of that tube raised to the power of a constant c that ranges between 2 and 3 ($Q = Kr^c$). In the special case where c was equal to 3 (Murray's law), a set of fluid-dynamics consequences would derive. In particular, our cost function reflects the concept that if c was equal to 3, wall shear stress (WSS) would be constant along each individual tree.

C. 0-D vascular model

A 0-D model was created to simulate the fluid-dynamics within the network. At the branching nodes, the conservation of mass was assumed. Therefore, at each bifurcation, the inflow of blood at the inlet matched the outflow from the outlet ($\sum_{(k=p,d_1,d_2)} \boldsymbol{Q_{j,k}} = 0$), where p, d_1, d_2 refer to the parent branch and the two child branches of the bifurcation respectively. By adopting H-P's law, $\boldsymbol{Q}$ was computed as ($Q_{jk} = G_{jk} \cdot \Delta P_{jk}$) in which the subscripts j and k refer to the circuit's nodes as shown in Fig. 2. The nodal pressure was computed by applying the conservation law, and solving the system of linear equations $\boldsymbol{Q} = \boldsymbol{G} \cdot \Delta \boldsymbol{P}$ (Eq. (3)). This system is in the form $\boldsymbol{Ax} = \boldsymbol{B}$, where $\boldsymbol{A}$ is the conductance matrix of size $n \times n$, with n number of the circuit's nodes, $\boldsymbol{x}$ and $\boldsymbol{B}$ are both $n \times 1$ vectors. The system can be solved if the matrix $\boldsymbol{A}$ is invertible. Such reversibility is ensured by adding a smoothing term $\epsilon = 1 \times 10^{-20}$ to $\boldsymbol{A}$. By solving this equation, the pressure values at each node of the circuit are computed. In this paper, each candidate tree was treated as arterial tree. To compute the fluid-dynamic parameters, at the inlets a

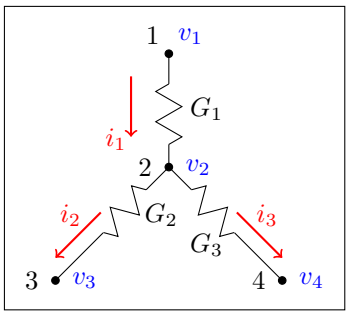

Fig. 2: An electric circuit of lumped elements. The numbers denote the nodes, v denotes nodal voltages; i currents; G the conductances. The red arrows point towards the current flow direction.

pressure value of 40 mmHg, which reflects the hydrostatic and frictional pressure losses from the aorta to the Central Retinal Artery (CRA) (Causin *et al.* [16]), was specified. To prevent vessels from collapse, a pressure slightly higher than the intraocular pressure in normal conditions (15 mmHg) was enforced at the outlet.

$$\begin{bmatrix} 1 & 0 & 0 & 0 \\ G_1 & -\sum_{i=1}^{3} G & G_3 & G_4 \\ 0 & 0 & 1 & 0 \\ 0 & 0 & 0 & 1 \end{bmatrix} \cdot \begin{bmatrix} P_1 \\ P_2 \\ P_3 \\ P_4 \end{bmatrix} = \begin{bmatrix} P_{in} \\ 0 \\ P_{out3} \\ P_{out4} \end{bmatrix} \quad (3)$$

D. Optimization problem: connect the segments

The vascular segments were connected by solving an optimization problem. A search for the optimal solution was conducted using a simulated annealing (SA) algorithm. SA is a meta-heuristic method commonly employed to solve unconstrained and bound-constrained optimization problems and find the global minimum of a function in large and discrete search space, while avoiding local minima. The following internal parameters were used:

- Probability of accepting a worse solution at the beginning: $P_{start} = 0.5$.
- Probability of accepting a worse solution at the end: $P_{end} = 0.001$.
- Equation of the temperature (T) trend, related to the probabilities of accepting a worse solution: $T_{start} = \frac{-1}{log(P_{start})}$; $T_{end} = \frac{-1}{log(P_{end})}$.
- Number of steps performed during cooling: N_{cycles} = 50.
- Number of possible solutions evaluated at each cycle: N_{trials} = 50.
- Fractional temperature reduction at every cycle: $\Delta T = (\frac{t_{end}}{t_{start}})^{(\frac{1.0}{N_{cycles} * N_{trials} - 1.0})}$.

III. RESULTS

The algorithm was tested on a subset of six images from the DRIVE test set: two left eye macula centered (images 1 and 5), two right eye macula centered (images 7 and 8) and two ONH centered (images 4 (right eye) and 15 (left eye)). The performance was evaluated by calculating the success rate in connecting each segment-end. We consider that a failure occurs in a situation in which two of the three members of a bifurcation were bridged, or a situation in which two bridging segments in the reference dataset were joined to a third segment-end to form a false bifurcation.

A. Evaluation

The evaluation of the connectivity success rate was evaluated in networks of different sizes: small (including up to 5 segments), medium (including up to 20 segments) and large (including more than 20 segments).

1) Small networks: In Fig. 3, 4 and 5, samples of solved small disconnected networks are shown. In Fig. 3-left, a crossing point is correctly identified and its cost is compared to a wrong configuration (Fig. 3-right). Fig. 4 and 5 report two samples of networks which consisted of 5 segments. With regard to Fig. 4-top, which is the correct configuration, we observed that the cost of this configuration, is more expensive than one which is incorrect (bottom). While in this sample the success rate of our algorithm was 0% in Fig. 5 the success rate is 100%. This discrepancy in the performance demonstrates that the fluid-dynamics, since it is a global feature, can barely discriminate among correct and wrong configurations in very small networks. In fact, in these networks, the configuration is strictly influenced by the diameter of the vessels of which the accuracy depends on the segmentation at disposal.

2) Medium-size networks: In Fig. 6, we observe that the correct configuration (top), does not always correspond with the less expensive configuration (bottom). The overall success rate is 85.2%.

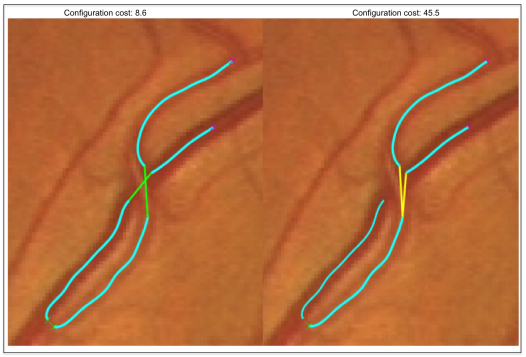

Fig. 3: Green dashes represent the connection between segments; yellow dashes represent bifurcations. **Left**: Crossing between 2 vessels. **Right:** A different configuration for the same network. Our cost function recognized the correct configuration (left) as the less expensive.

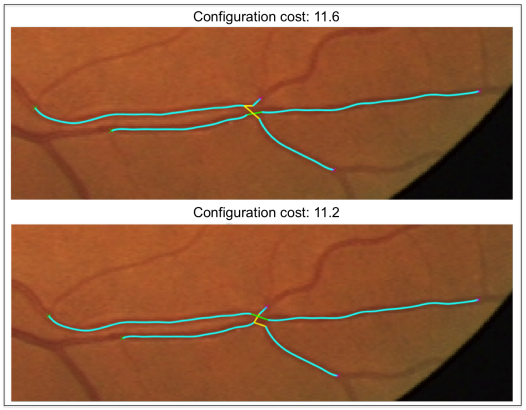

Fig. 4: **Top**: The correct configuration. **Bottom:** The less expensive configuration according to our cost function.

3) Large networks: In large networks, we manually tested our cost function by comparing the cost of the correct configurations (Fig. 1-top) with some other plausible configurations. The former were derived by visually inspecting the artery and vein ground truth proposed by Qureshi *et al.* [9]. The latter were obtained by connecting a number of segment-ends to wrong end-candidates. For each image, 30 different plausible networks were generated. In Fig. 7 an example of plausible solutions, related to the image 4 is shown. We use the adjective plausible because also a human expert would find establishing the correct connectivity difficult. As shown in Fig. 1-bottom, for the image 1, the minimum cost was found on a network with success rate of 98.95%. With regard to images 4, 5, 7, 8 and 15, the costs of the correct configurations were: 20.77, 11.89, 18.81, 31.54, 24.81. The minimum costs observed among the candidate networks were: 16.37, 10.23, 18.74, 28.50, $24,79$. The success rates were 98.8%, 98.7%, 97.7%, 97.5% and 98.8% respectively. The increase of the success rate achieved on large networks in all the tested images, demonstrates that the connectivity is a global problem and our cost function, which is based on fluid-dynamic concepts is able to capture the global behaviors of the system.

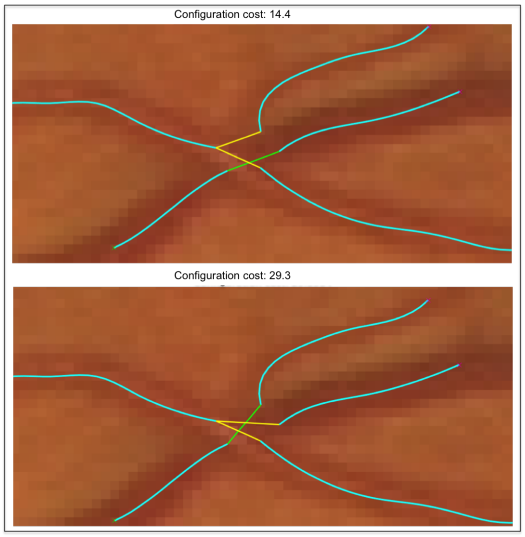

Fig. 5: **Top**: The correct configuration. **Bottom:** A different configuration for the same network. Our cost function recognized the correct configuration (left) as the less expensive.

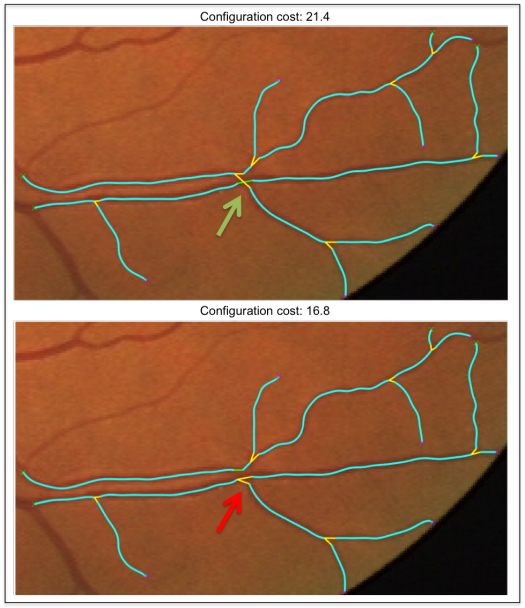

Fig. 6: **Top**: The correct configuration. The green arrow points toward a bifurcation and a vessel crossing that were not correctly recognized in the optimal configuration (red arrow in the image located at the bottom). **Bottom:** The less expensive configuration according to our cost function.

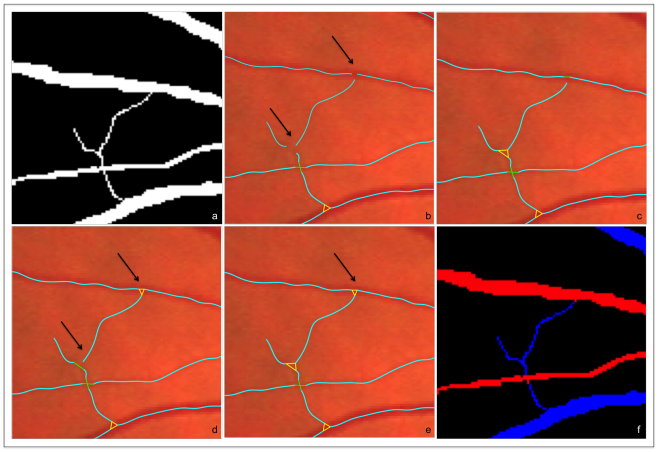

Fig. 7: **a:** A portion of the first manual vessel reference standard of the image 4 of DRIVE test set. **b:** Vessels' centerlines obtained by applying the morphological skeletonization to (**a**). Some segments have already been connected to form a bridge (green dash line) and a bifurcation (yellow line). The arrows point towards the segments' ends, of which the correct connectivity is difficult to be established. **c:** The correct configuration ascertained by visually inspecting (**f**). Same type of vessel should be joined together: artery with artery, vein with vein. **d:** A plausible wrong configuration. The two arrows point towards a wrong bridge and bifurcation. **e:** A plausible wrong configuration. The arrow point towards a wrong bifurcation. **f:** The artery/vein ground truth of (**a**)

IV. CONCLUSIONS

In this paper, a novel algorithm to reconstruct the retinal vascular network from the segmentation of fundus images was presented. A 0-D model was created to simulate the fluid-dynamic conditions within each vascular network. Our algorithm uses a novel fluid-dynamics based cost function to derive fluid-dynamic terms, which are not directly retrievable from standard fundus images, and employs them, to assess candidate configurations of retinal vascular trees. A simulated annealing algorithm was implemented to search for the optimal trees. Evaluation was performed on a subset

of DRIVE test set, nevertheless, we intend to extend the validation of our methodology to other higher resolution and publicly available datasets. The accuracy of the results achieved shows that while increasing the size of the network, the success rate of the framework increases, as the cost function is targeted at studying the global behavior of the network. A further development of the presented framework would include an algorithm able to automatically classify the extracted trees as either arterial or venous. To conclude, the performance and simplicity of the presented model makes it applicable in the automation of longitudinal studies in which comparisons among hemodynamic conditions are required.

ACKNOWLEDGMENT

This research was made possible by a Marie Curie grant from the European Commission in the framework of the RE-VAMMAD ITN (Initial Training Research network), Project number 316990.

REFERENCES

[1] Balvinder Wasan, Alessia Cerutti, Susan Ford, and Ronald Marsh. Vascular network changes in the retina with age and hypertension. *Journal of hypertension*, 13(12):1724–1728, 1995. Face and Gesture submission ID 324. Supplied as additional material `fg324.pdf`.

[2] Alun D Hughes, Elena Martinez-Perez, Abu-Sufian Jabbar, Assif Hassan, Nick W Witt, Paresh D Mistry, Neil Chapman, Alice V Stanton, Gareth Beevers, Roberto Pedrinelli, et al. Quantification of topological changes in retinal vascular architecture in essential and malignant hypertension. *Journal of hypertension*, 24(5):889–894, 2006.

[3] Muhammad Bayu Sasongko, Jie Jin Wang, Kim C Donaghue, Ning Cheung, Paul Benitez-Aguirre, Alicia Jenkins, Wynne Hsu, Mong-Li Lee, and Tien Y Wong. Alterations in retinal microvascular geometry in young type 1 diabetes. *Diabetes Care*, 33(4):1331–1336, 2010.

[4] Diego Marín, Arturo Aquino, Manuel Emilio Gegúndez-Arias, and José Manuel Bravo. A new supervised method for blood vessel segmentation in retinal images by using gray-level and moment invariants-based features. *IEEE transactions on medical imaging*, 30(1):146–158, 2011.

[5] Muhammad Moazam Fraz, Paolo Remagnino, Andreas Hoppe, Bunyarit Uyyanonvara, Alicja R Rudnicka, Christopher G Owen, and Sarah A Barman. An ensemble classification-based approach applied to retinal blood vessel segmentation. *IEEE Transactions on Biomedical Engineering*, 59(9):2538–2548, 2012.

[6] George Azzopardi, Nicola Strisciuglio, Mario Vento, and Nicolai Petkov. Trainable cosfire filters for vessel delineation with application to retinal images. *Medical image analysis*, 19(1):46–57, 2015.

[7] Qiaoliang Li, Bowei Feng, LinPei Xie, Ping Liang, Huisheng Zhang, and Tianfu Wang. A cross-modality learning approach for vessel segmentation in retinal images. *IEEE transactions on medical imaging*, 35(1):109–118, 2016.

[8] Sherman, Thomas F. On connecting large vessels to small. The meaning of Murray's law. *Journal of general physiology*, 78(4):431–453, 1981.

[9] Touseef Ahmad Qureshi, Maged Habib, Andrew Hunter, and Bashir Al-Diri. A manually-labeled, artery/vein classified benchmark for the drive dataset. In *Proceedings of the 26th IEEE International Symposium on Computer-Based Medical Systems*, pages 485–488. IEEE, 2013.

[10] Marta Favali, Samaneh Abbasi-Sureshjani, Bart Haar Romeny, and Alessandro Sarti. Analysis of vessel connectivities in retinal images by cortically inspired spectral clustering. *Journal of Mathematical Imaging and Vision*, 56(1):158–172, 2016.

[11] Rolando Estrada, Michael J Allingham, Priyatham S Mettu, Scott W Cousins, Carlo Tomasi, and Sina Farsiu. Retinal artery-vein classification via topology estimation. *IEEE transactions on medical imaging*, 34(12):2518–2534, 2015.

[12] Qiao Hu, Michael D Abràmoff, and Mona K Garvin. Automated construction of arterial and venous trees in retinal images. *Journal of Medical Imaging*, 2(4):044001–044001, 2015.

[13] Joes Staal, Michael D Abràmoff, Meindert Niemeijer, Max A Viergever, and Bram van Ginneken. Ridge-based vessel segmentation in color images of the retina. *IEEE transactions on medical imaging*, 23(4):501–509, 2004.

[14] Cecil D Murray. The physiological principle of minimum work i. the vascular system and the cost of blood volume. *Proceedings of the National Academy of Sciences*, 12(3):207–214, 1926.

[15] Cecil D Murray. The physiological principle of minimum work applied to the angle of branching of arteries. *The Journal of general physiology*, 9(6):835–841, 1926.

[16] Causin, P., Guidoboni, G., Malgaroli, F., Sacco, R., and Harris, A. Blood flow mechanics and oxygen transport and delivery in the retinal microcirculation: multiscale mathematical modeling and numerical simulation. *Biomechanics and modeling in mechanobiology*, 15(3):525–542, 2016.